Enhanced photovoltaic performance of dye sensitized solar cell based on nanocomposites of zinc oxide photoanode

A. V. Balan [a1], P. Gopinath [a], V. Radhika [b]
[a] *Department of Mechanical Engineering, KSR College of Engineering, Tiruchengode, Tamilnadu,*
[b] *Associate Professor, Department of EIE, Sri Ramakrishna Engineering College, Coimbatore*

XRD and SEM images of ZnO nanoparticles prepared by the precipitation method allow investigation of their morphology and morphological refinement. No contamination was observed in the XRD spectrum and SEM confirmed that the nanoparticles were well-coordinated ZnO at 30 nm size. UV-Vis spectroscopy was used to tune the optical properties and they appeared not to be fixed at 3.34 eV. The band gap of semiconductor materials makes them competitive for solar cell applications. The O-rich stoichiometry measured by XPS may be a direct result of zinc deficiency. Therefore, ZnO nanoparticles were prepared to fabricate secretory solar cells (DSSCs). From the perspective of J-V, open circuit voltage (Voc), barrier thickness (Jsc), fill factor (FF) and efficiency (η) were not chosen as much as possible and the quality was calculated as 0.65V, 6.26mA. , 62.2% and 1.96% respectively at 100mW/cm^2.

(Received September 19, 2023; Accepted January 15, 2024)

Keywords: ZnO, DSSC, TEM, XPS

1. Introduction

In recent years, Zn-O photoanodes have emerged as an appealing alternative. Zn-O is a photoelectrode material having a wide energy band gap, similar to Ti-O_2 in this regard. Zn-O is used in DSSCs due to the fact that it has advantageous crystallisation and electrical conduction capabilities. Zn-O has the potential to be fashioned into a wide variety of nanostructures with very little effort. Additionally, the electron mobility of Zn-O ranges from 110 to 150 $cm^2V^{-1}s^{-1}$, which is 7 orders of magnitude higher than the electron mobility of Ti-O_2, which is 10^{-5} $cm^2V^{-1}s^{-1}$. Both kinds of electrodes exhibit kinetics of electron injection and recombination that are equivalent under conditions of operation that are comparable to one another. Zn-O has been the focus of a significant amount of research because of the possibility that it may be used in DSS-Cs; nevertheless, the conversion efficiencies that have been reported for ZnO-based DSSCs are not nearly as high as those for DSS-Cs that use Ti-O_2 photoelectrodes. Since the Zn-O nanoparticles we prepared have a wide bandgap, they can act as semiconductors and we exploit this property to form DSSCs. Curiously, DSSC was first described by O'Regan and Gratzel [1] and has since become one of the most effective energy-saving systems of all time. A strong and appropriate force is urgently needed in this world to make the best of our progress. DSSC is the best way to meet huge electricity demand. Due to their simple manufacturing processes, low collection costs and environmental friendliness, DSSCs have attracted researchers in recent years [2].Due to their wide bandgap and low exciton retention at ambient temperature, ZnO nanoparticles may be the most likely candidates for the fabrication of state-of-the-art DSSCs. DSSCs with high-performance photoanodes still have room for improvement. Ratnasamy et al. [3] adopted a method to synthesize hexagonal wurtzite ZnO nanoparticles. ZnO nanoparticles were used as photoanodes in shade-optimized solar control cells and increased energy conversion by 1.6% Additionally, Sharma et al.

[1]Corresponding author: balanavksr@gmail.com
https://doi.org/10.15251/JOR.2024.201.85

[4] used ZnO nanoparticles as the photoanode of photosensitive solar cells and achieved an efficiency of 0.66%. While the use of ZnO nanoparticles produced by chemical synthesis to produce DSSCs has been explained by some experts, the use of nanoparticles produced by conventional methods to produce DSSCs has been described as very limited. In this work, we successfully developed ZnO nanoparticles and their use in DSSCs as part of a loop model.Also, the overwhelmingly positive respect they received (1.96%) is greater than the ratings given on television.

2. Experimental work

2.1. Strategy of ZnO nanoparticles

Zinc nitrate hexahydrate [$Zn(NO_3)_2.6H_2O$], sodium hydroxide (NaOH), Triton-X 100 and acetylacetone were purchased from Sigma-Aldrich. Integration of the 0.2M zinc nitrate hexahydrate concept with 2.972 g of salt in a 100 mL standard vessel using twice as much clean water. Mix the mixture in a blender at room temperature for 5 minutes to obtain a homogeneous relationship. 0.5M NaOH was then added dropwise and stirring continued at 70°C for 1-5 minutes to complete precipitation. The reaction was cooled to room temperature and the sample was centrifuged at 6500 rpm for 15 minutes. Kill the supernatant and wash with water and spin again. Afterwards, after various centrifugation processes, free zinc oxide nanoparticles were placed on the observation glass and dried for a while in a chicken rotisserie oven at 70°C.

2.2. Fabrication of ZnO-based DSSC

The same approach was used to coat indium tin oxide (ITO) with ZnO nanopowders, which had an area of 0.25 cm^{-2}. To make the coating, combine the ZnO nanopowder with a paste using a pestle, distilled water, acetylacetone, and Triton-X 100. To create a ZnO film, the slurry was blade-extruded onto the ITO surface. To get rid of any organic residues, the films were heated to 450°C for two hours. A solution of 0.2 mM N719 ((cis-diisothiocyanato-bis(2,2'-bipyridyl-4,4'-dicarboxy)ruthenium(II)bis(tetrabutylammonium):ruthenizer 535 bis-TBA, Solaronix Co.) was used to put the annealed layer. After two hours of darkness at room temperature, the dye was rinsed with methanol and allowed to dry. Research has demonstrated that the resulting photoanode exhibits a reddish-red hue. Making use of sealing tape to avoid short circuits, a sandwich-type DSSC is created by clamping a platinum-coated counter electrode to the dye-impregnated ZnO sheet. Then the device was filled with redox electrolyte (Iodolyte AN-50, Solaronix Co.) through the gap between the counter electrodes for DSSC generation.

3. Result and discussion

3.1. XRD analysis

The X-ray diffraction (XRD) representation of coordinated ZnO nanoparticles is shown in Figure 1. The diffraction peaks at 2θ at 31.71°, 34.37° and 36.22° are freely correlated with the (100), (002) and (101) plane and confirmed the planar activity of ZnO (Zincite) by the hexagonal process. Each specific peak is prepared according to the JCPDF card number: 361451. The diffraction peaks of the integrated ZnO nanoparticles are elongated after calcination as they preserve the nanostructure [5, 6 The apex development is also caused because of high strain, instrumental screws up, and so forth [7]. We use the Scherrer relationship to find the bulk culture of ZnO nanoparticles [8];

$$D = 0.9\lambda/\beta \cos\theta \quad (1)$$

D is a typical crystallite size, K is defined as a constant equal to 0.94, λ is the X-ray radiation (0.154 nm), γ is the full-width half-limit of the top (in radians), and 2θ is Bragg's point (in degrees). The size of the crystallite was not fixed for diffraction peaks (100), (002), and (101) according to Scherrer's criterion, and the standard size was considered to be 12 nm. The cross-

sectional dimensions were carefully measured and found to be a=3.25æ, b=3.25æ, and c=5.21å, with the centre of the structure being α=90˚, β=90˚, and γ= 120˚.

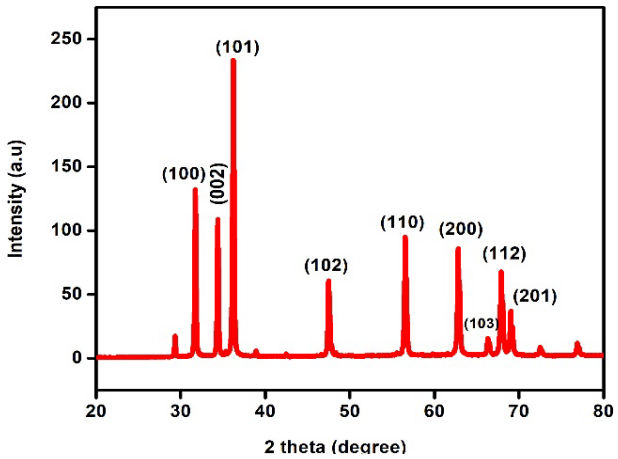

Fig. 1. Powder X-ray diffraction pattern of synthesized ZnO nanoparticles.

3.2. FTIR analysis

Fourier Transform Infrared Spectroscopy (SHIMADZU - FTIR 8400) examination validated the kind of connection between the metal atoms and metal atoms with oxygen. Figure 2 depicts the FTIR spectrum of ZnO nanoparticles generated in a laboratory. The O-H stretching and bending frequencies were found to be responsible for the abrupt intensity peaks at 3445 cm-1 and 1634 cm-1. EDAX and XRD examination confirmed the development of zinc oxide, with the presence of a peak at 450-850 cm-1 corresponding to the Zn-O metal oxide. Intermolecular interaction between zinc metal atoms and oxygen atoms in zinc oxide is responsible for the 2426 cm-1 peaks. The ZnO showed characteristically sharp peaks, confirming its crystalline structure. In addition to the creation of zinc oxide, no other peaks were seen, indicating that no contaminants were present throughout the reaction.

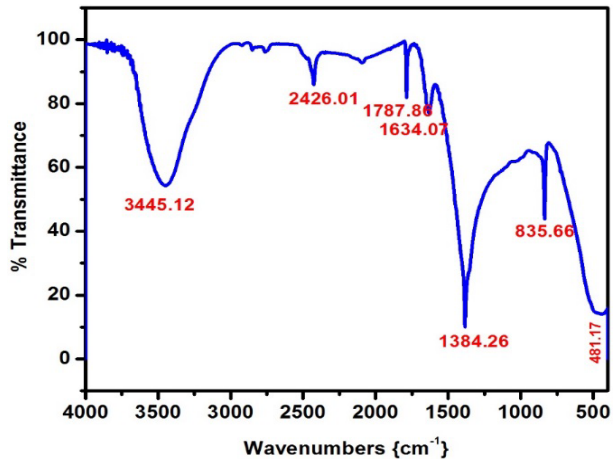

Fig. 2. FTIR analysis of synthesized ZnO nanoparticles.

3.3. SEM/EDAX analysis

Figure 3(a) shows the SEM microstructure of ZnO nanoparticles. The SEM microstructure describes the proportional reflection of mixed nanoparticles. The size and shape of ZnO nanoparticles is about 32 nm and is rod-like. The planned ZnO nanoparticles have little aggregation due to their small size and homogeneous properties. It is not utilized costly and destructive covering specialists to lessen agglomeration regardless, it goes most likely as both diminishings prepared proficient and covering prepared proficient. Hence, this methodology is more moderate and eco-obliging than some various strategies for organizing ZnO nanoparticles. TEM morphology spectrum fabricated ZnO NPs were depicted in Fig-3 (b). It shows the long-scale-like morphology of the component. The long-scale morphological compound has an enhanced optical plasmonic effect with the help of dye-sensitized solar cells. EDS analysis of ZnO nanoparticles, shown in Figure 3 (c), was used to identify their specific molecular structure. An immense portion of each was considered to be the value, and the nuclear amount of zinc was not fixed hypothetically. At its core, zinc's nuclear level was not completely established logically, and its features were considered crucial to both. In agreement with the predicted characteristics, the EDS results show that the oxygen and zinc in the supported ZnO nanoparticles are stoichiometric with regard to one another.

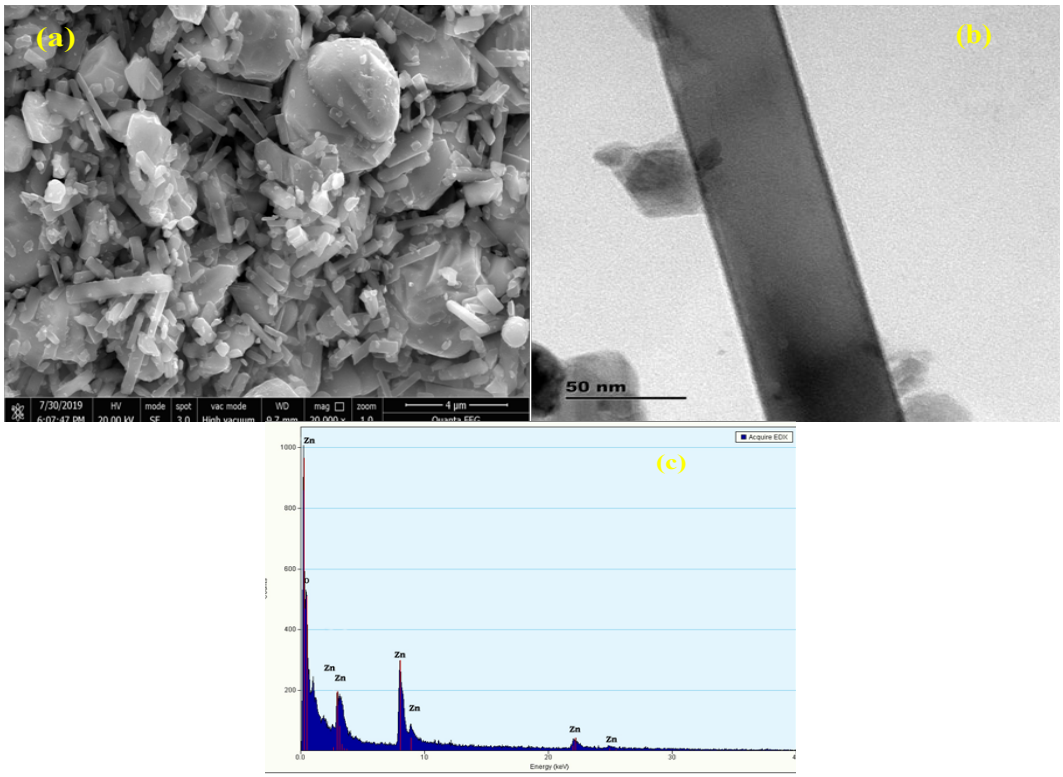

Fig. 3. (a) FE-SEM of ZnO (b) TEM profile of ZnO rod (c) EDS composition of ZnO NPs

3.4. Ultraviolet-visible spectroscopy and bandgap calculation

ZnO nanoparticles' band gap was calibrated by means of UV-Vis spectroscopy. Using a sonicator, evenly distribute the small ZnO nanoparticles in deionized water for a precise alignment. The produced ZnO nanoparticles' UV transparency degree is displayed in Figure 4a. As a direct result of surface plasmon absorption by ZnO nanoparticles, they have arrived, and their arrival peak is broad at 295 nm. Because free conduction band electrons oppose each other when exposed to electromagnetic radiation, surface plasmon absorption becomes eccentric [9, 10]. The current study's UV Visible ingestion peak for ZnO nanoparticles is quite unclear and contradictory with other results. This brand-name bandgap (Figure 4b) in ZnO is the result of electron transitions

from the valence band to the conduction band, and their band opening energy respect is still 3.34 eV. Clinical uses for ZnO nanoparticles include sunscreen shields and clean medications, made possible by their absorption at the UV site[11].

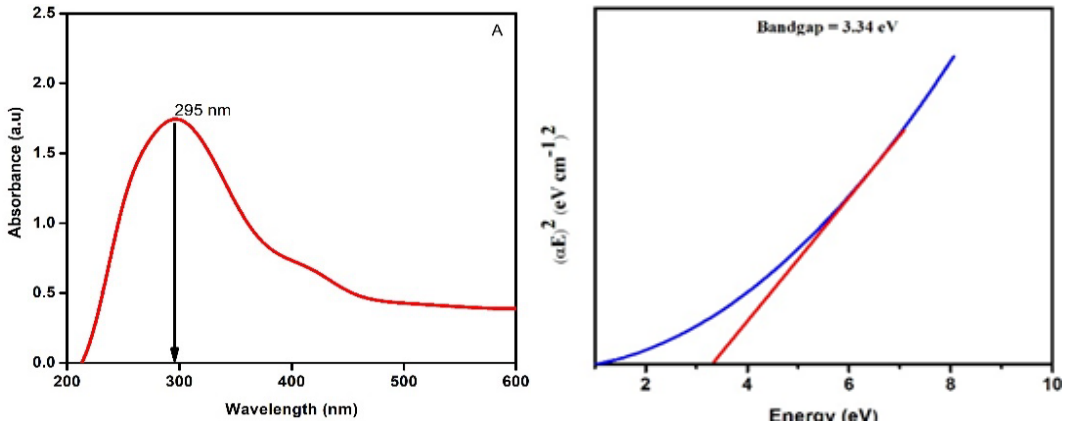

Fig. 4. UV spectra (a) and Bandgap(b) Prepared ZnO NPs.

3.5. XPS analysis

XPS Survey spectrum, d convoluted curve and XPS scan of Zn 2p and O 1s core levels as shown in Figure 5(a), 5(b) and 5 (c) respectively.

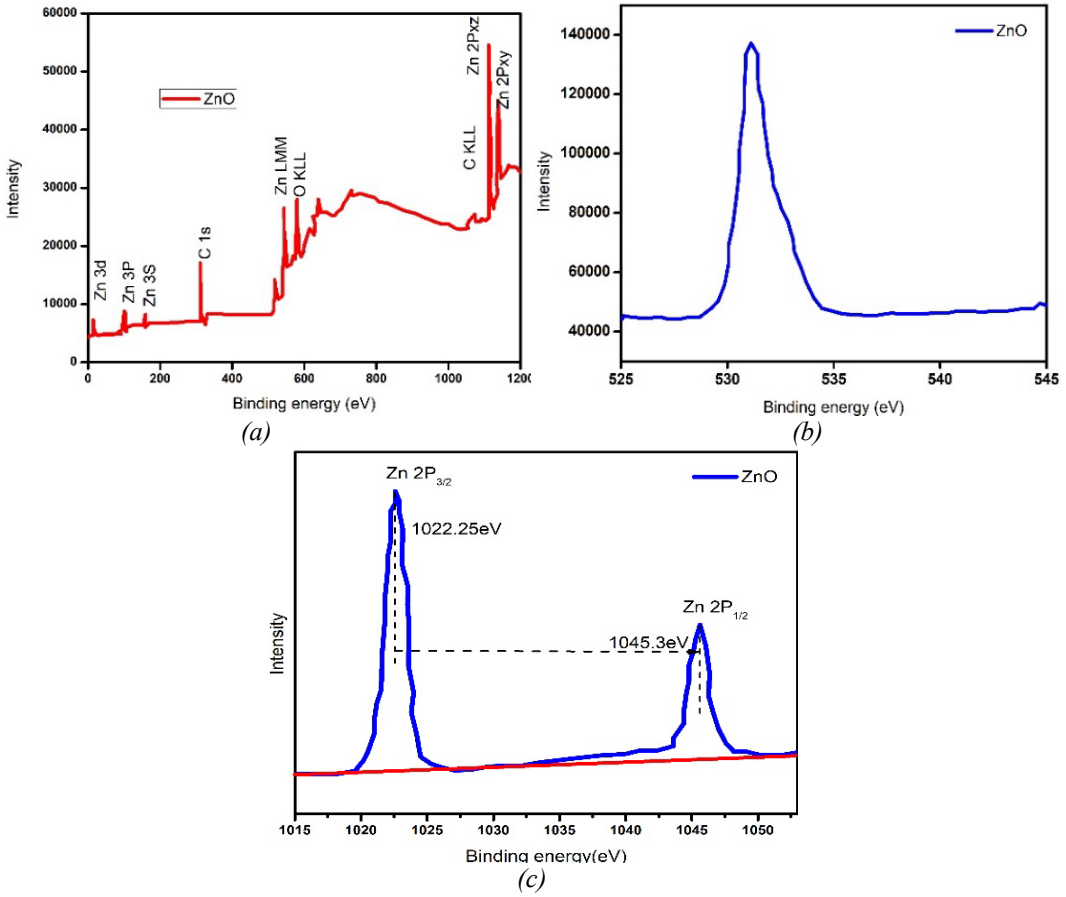

Fig. 5. a) XPS survey Spectrum b) d convoluted curve and c) stimulated core level spectrum.

The Zn 2p3/2 and 2p1/2 emissions centered at 1022.25eV and 1045.31eV found to be separated by B.E. value of 23.06eV. This also implies the formation of ZnO. In survey spectrum of ZnO, an Auger Zn L3M4, 5M4,5 emission at 497.49 eV is also detected and attributed to interstitial Zn–O bonds. The peak at 493.8eV, earlier reported for Zni, is absent in our case. This suggests that synthesized ZnO nanoparticles are lacking Zni defects and therefore, Zn deficient condition could consequently give rise to O rich stoichiometry. Further, deconvolution of O 1s line shape reveals three distinct peak profiles centered respectively at 530.23 eV, 531.57eV, and 532.60eV. As per literature, the low (at 530.23eV), medium (at 531.57 eV) and high (at 532.60eV) are attributed respectively to lattice site oxygen (OL), VO and Oi.

3.6. Electrical depiction of ZnO-based DSSC

The fill variable of DSSC can be controlled by

$$FF = Jmax \times Vmax / Jsc \times Voc \tag{2}$$

where Jmax, Vmax, JSC, and VOC stand for the maximum current and voltage gains at the most extreme powerpoint, zero-volt conscious current, and open-circuit voltage, respectively. According to the current state of affairs, the power change capability (n%) is defined as the distance between the maximum power (Pmax) and the electrical data power (Pin);

$$\eta = FF \times Voc\ xJsc / sxPln \tag{3}$$

DSSC space is denoted by S [12]. As seen in Figure 6, DSSCs based on ZnO exhibit current-thickness voltage (J-V) distortion across optic powers. Open circuit voltage (Voc), barrier thickness (Jsc), and fill factor (FF) are the three variables that DSSC restricts in relation to J-V distortion; nonetheless, (2) and (3) seldom dictate competence. Table 1 provided the still-uncertain possible advantages of DSSC limitations. The n% value of the manufactured ZnO-based DSSC was deemed very different from the tests conducted using comparable ZnO nanoparticle architectures in the previous work [13]. The sun-situated cell limitations of the ZnO-based DSSC are supposedly heavily reliant on the diving duration of a ZnO film into an honing tone [14]. In contrast to previous studies, the transmitted ZnO-based DSSC demonstrated improved vitality in a shorter period of immersion time [15]. Another possible explanation for the enhanced capacity is the prolonged absorption due to the increased amount of shade particles adsorbed onto the ZnO surface. Consequently, the direct and easily manufactured ZnO nanoparticles for usage in photovoltaics are an encouraging development for the future. The present level of thickness was considered to be quite low. In order to find out how efficient the system may become, the photocurrent is the most important parameter. If it is successful in controlling nanoscale atomic mass, the parent material's large surface area and surface energy will lead to desirable outcomes [16–18].

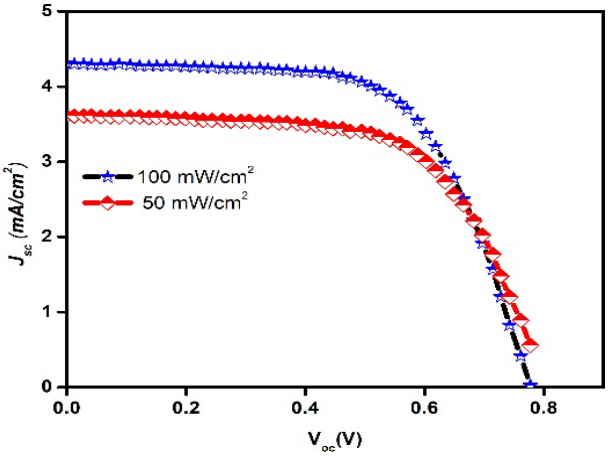

Fig. 6. J-V graph of fabrication of ITO/ZnO NPs on dye-sensitized solar cells.

The grain size of organized ZnO nanoparticles is about 22 nm; therefore, we can expect a large amount of energy. Many factors can cause low photocurrents, such as small changes, reflections or bursts from the photoanode, insufficient mixing and charge sources [19].

Value of the short-out current directly increased to the properties near saturation as the light power increased. The rapid improvement in (Jsc) was thought to be due to increased photogenerated excitons [20]. Thus, under stronger light sources, a greater number of electron densities were transferred to ZnO. Table 1 shows that when the applied light thickness increases, n and Jsc become more stretched. As a result of an increase in control age, light power has been augmented. The ZnO-based DSSC has achieved near-insightful results. These findings demonstrate that transport, imbuement, and recombination frameworks remain unchanged when the light power is increased up to 100 mW/cm^2.

Table 1. Photovoltaic parameters of ZnO NPs.

Intensity (mW/cm^2)	J_{sc} (mA/cm^2)	V_{oc} (V)	n (%)	FF (%)
50	3.84	0.60	1.32	38.3
100	4.36	0.68	2.09	62.2

4. Conclusion

Precipitation was an effective procedure for preparing the ZnO nanoparticles. The coordinated ZnO nanoparticles displayed a single-stage hexagonal growth with a typical crystallite size that could not be determined from Scherrer's equation. The nanoparticles were found to be rod- and long-shaped with little aggregation, as shown by SEM/TEM analysis. However, the NaOH integration separates itself probably as both decreasing sizes similarly to doping, so we did not use any extra doping agents to reduce agglomeration in this investigation because of their toxic character.

Therefore, compared to other methods for organizing ZnO nanoparticles, this method is more efficient and environmentally friendly. The size of ZnO nanoparticles is 80 nm. EDS analysis confirmed the theoretical and possible stoichiometric ratio of zinc to oxygen. As seen in the UV-Vis spectrum, ZnO nanoparticles have a wide bandgap of 4.2 eV and an absorption peak at 295 nm due to surface plasmon resonance. Using a current thickness voltage lead, the DSSCs comprised of ZnO nanoparticles were successfully fabricated, and their display was evaluated in

the dark using artificial light. An enormous increase in the preservation of shading iotas onto the outer layer of ZnO nanoparticles is responsible for the great utility of the manufactured DSSC. Therefore, manufacturing DSSC with ZnO nanoparticles is a simple and promising future-proofing technique.

References

[1] B. O'Regan, M. Grätzel, Nature, 353 (1991) 737-740; https://doi.org/10.1038/353737a0

[2] F. Shao, J. Sun, L. Gao, S. Yang, J. Luo, J. Phys. Chem. C. 115 (2011) 1819-1823; https://doi.org/10.1021/jp110743m

[3] R. Rathnasamy, P. Thangasamy, R. Thangamuthu, S. Sampath, V. Alagan, J Mater Sci: Mater Electron. 28 (2017) 10374-10381; https://doi.org/10.1007/s10854-017-6807-8

[4] J.K. Sharma, P. Srivastava, G. Singh, M.S. Akhtar, S. Ameen, Materials Science and Engineering: B, 193 (2015) 181-188; https://doi.org/10.1016/j.mseb.2014.12.012

[5] R. Shashanka, D. Chaira, Mater Charact. 99 (2015) 220-229. 15; https://doi.org/10.1016/j.matchar.2014.11.030

[6] M.S Manojkumar, K. Jeyajothi, A. Jagadeesan. V. Jeevanantham, Journal of the Indian Chemical Society. 99((2022), 100559. https://doi.org/10.1016/j.jics.2022.100559

[7] V. Jeevanantham, D. Tamilselvi, K. Rathidevi, & S. R Bavaji, Journal of Materials Research, 38((2023), 1909-1918. https://doi.org/10.1557/s43578-023-00965-3

[8] S. Arul, T. Senthilnathan, V. Jeevanantham, K.V Satheesh Kumar, Archives of Metallurgy and Materials, 66(2021), 1141-1148.

[9] R. Shashanka, B.E.K. Swamy, Physical Chemistry Research, 8 (1) (2020) 1-18; https://doi.org/10.30723/ijp.v18i46.559

[10] R. Shashanka, Y. Kamacı, R. Taş, Y. Ceylan, A.S. Bülbül, O. Uzun, A.C. Karaoglanli, Physical Chemistry Research, 7 (4) (2019) 799-812.

[11] Q. Zhang, C.S. Dandeneau, X. Zhou, G. Cao, Adv. Mater. 21 (41) (2009) 4087-4108; https://doi.org/10.1002/adma.200803827

[12] A.E. Suliman, Y. Tang, L. Xu, Solar Energy Materials and Solar Cells, 91 (18) (2007) 1658-1662; https://doi.org/10.1016/j.solmat.2007.05.014

[13] E. Guillén, F. Casanueva, J.A. Anta, A. Vega-Poot, G. Oskam, R. Alcántara, C. Fernández-Lorenzo, J. Martín-Calleja, Journal of Photochemistry and Photobiology A: Chemistry, 200 (2-3) (2008) 364-370; https://doi.org/10.1016/j.jphotochem.2008.08.015

[14] R. Rathnasamy, P. Thangasamy, R. Thangamuthu, S. Sampath, V. Alagan, J Mater Sci: Mater Electron. 28 (2017) 10374-10381; https://doi.org/10.1007/s10854-017-6807-8

[15] V. Jeevanantham, D. Tamilselvi, K. Rathidevi, S. R Bavaji, P. Neelakandan, Biomass Conversion and Biorefinery, (2023)1-10. https://doi.org/10.1007/s13399-023-04179-9

[16] P. Gopinath, P. Suresh, V. Jeevanantham, Journal of Ovonic Research, 19 (2023). https://doi.org/10.15251/JOR.2023.191.23

[17] R. Shashanka, J.W. Elam, J.T. Hupp, M.J. Pellin, ZnO Nanotube-Based Dye Sensitized Solar Cells, Nano Letters, 7 (8) (2007) 2183-2187; https://doi.org/10.1021/nl070160+

[18] B. Pradhan, S.K. Batabyal, A.J. Pal, Solar energy materials and solar cells, 91 (9) (2007) 769-773; https://doi.org/10.1016/j.solmat.2007.01.006

[19] A.K. Nayak, R. Shashanka, D. Chaira, IOP Conf. Series: Materials Science and Engineering, 115 (2016) 012008; https://doi.org/10.1088/1757-899X/115/1/012008

[20] S. Gupta, R. Shashanka, D. Chaira, IOP Conf. Series: Materials Science and Engineering, 75 (2015) 012033; https://doi.org/10.1088/1757-899X/75/1/012033